TECTONICS AND TOPOGRAPHY: CRUSTAL DEFORMATION, SURFACE PROCESSES, AND LANDFORMS

GEOLOGICAL SOCIETY OF AMERICA ANNUAL MEETING WORKSHOP, NOVEMBER 4, 2001 STRUCTURAL GEOLOGY AND TECTONICS DIVISION

WORKSHOP LEADERS:

Dr. Dorothy Merritts, Geosciences Department
Franklin and Marshall College, Lancaster, PA, 17604-3003
(717)291-4398, d_merritts@email.fandm.edu

Dr. Roland Bürgmann, Department of Earth and Planetary Science
University of California at Berkeley, Berkeley, CA 94720
(510)643-9545, burgmann@seismo.berkeley.edu

and Guest Lecturer Dr. Rudy Slingerland, Department of Geosciences
Penn State University, State College, PA 16802
(814)865-6892, sling@geosc.psu.edu

TECTONICS AND TOPOGRAPHY:
CRUSTAL DEFORMATION, SURFACE PROCESSES, AND LANDFORMS

General Greetings and Introductions (8:00-8:15)

I. Tectonics, Landscapes, and Landscape Evolution (8:15-9:30 AM)

A. Landscapes: Products of Tectonic and Geomorphic Forces

B. Fundamental Questions in Studies of Tectonics and Topography

C. Feedbacks between Mountain Building and Erosional Processes

Activity: Tectonics and Topography Earthscape Images

BREAK (9:30-9:45)

II. Recent Advances in Studies of Tectonics and Topography (9:45-10:45 AM)

A. Synopsis of Recent Advances

B. Mapping Global Topography and Deformation with Airborne and Space-Based Measurements

1. Global Positioning System

2. InSAR (Interferometric Synthetic Aperture Radar)

DISCUSSION/QUESTIONS (10:45-11:00)

III. Crustal Deformation and Landscape Generation (11:00 AM-12:00 PM)

A. Fault Scarps and Fault Slip: Morphological Features and Crustal Movements

B. Mountain-Building Along a Strike-Slip Fault

Exercise: Quaternary Sea-Level Change and Emergent Coral Terraces, New Guinea

LUNCH BREAK (12:00 - 1:00 PM)

IV. Numerical Modeling of Landscape Evolution (1:00-3:00 PM)

A. Introduction to Numerical Modeling and MATLAB

1. MATLAB Tutorial—data analysis and plotting

2. Gridding and trend-surface analysis of deformed wave-cut platforms along the San Andreas fault

B. Landscape Evolution: Tectonic Uplift, Sea-level Change, and Marine Terrace Generation (MATLAB finite-difference of R. S. Anderson)

C. Fault-Scarp Simulation: Generation and Degradation of Topography (MATLAB 'Penck' model of G. E. Hilley and J. Ramon Arrowsmith)

DISCUSSION AND QUESTIONS (3:00-3:15)

BREAK (3:15-3:30 PM)

V. Interactions between Crustal and Surficial Processes (3:30-4:30 PM)

A. Taiwan Case Study: Erosion, Climate, and Mountain Building (presented by Dr. Rudy Slingerland, Pennsylvania State University)

FINAL DISCUSSION AND QUESTIONS (4:30-5:00 PM)

I. Introduction: Tectonics, Landscapes, and Landscape Evolution (8:15-9:30 AM)

Landscapes can inspire reverence and wonder (Figure 1), leading Merritts and Ellis (1994) to suggest that "Landscapes are to field geologists what stars . . . [are to] . . . cosmologists." In the 19th and early 20th centuries, the origins of landscapes were the sources of great debates (e.g., William Morris Davis' peneplains), in part because the interior Earth was as yet inaccessible to study and global topography was incompletely mapped(see Chorley, 1963; Chorley et al., 1965).

Throughout the 20th century, the links and feedbacks between internal and external Earth processes, and the landscapes that result from their dynamic interactions, became increasingly better understood as a result of advances in plate tectonics, investigations on every continent (and other planets), and a variety of new technologies. Today, studies of the interactions between crustal and surficial processes are referred to as the field of "tectonics and topography", one that draws from a wide range of disciplines in Earth and planetary sciences.

FIGURE 1. The snow-capped Himalayan-Pamir Mountain Belt, along the borders of India, Pakistan, China, and Kyrgyzstan, is the roof of an ~80-km-thick welt of folded and faulted rocks formed as the Indian and Eurasian plates collide. (Image of Pamir Mountains from Arrowsmith and Strecker, 1999.)

A. Landscapes: Products of Tectonic and Geomorphic Forces

Prior to the plate tectonic revolution, Walther Penck noted that landscapes do not develop until "the earth's crust offers . . . surfaces of attack" (published in 1953). The early 20th century German geomorphologist realized that ". . . the problem [of landform origins] is that of crustal movement. . .", of which little was known at the time:

> "Crustal movements cannot be observed directly, and no adequate method is known for ascertaining their characteristics. . . . It is the crustal movements which correspond to the unknown, about which statements can be made only as a final result of the investigation, not as one of the premises. . . Morphological analysis is this procedure of deducing the course and development of crustal movements from the exogenetic processes and the morphological features." (p. 6, Penck, Walther, 1953, Morphological analysis of land forms, translated by Czech, Hella, and Boswell, Katherine Cumming: London, United Kingdom, MacMillan, 429 p.)

Penck realized that crustal and surficial processes are intimately linked to one another. He regarded the Earth's surface as "a field of reaction between opposing forces, and the effectiveness of one depends upon the preceding activity of the other" (1953, p. 6). Today, we recognize the prescience of the ideas of Penck and others, as modern researchers generate integrative, regional- to continental-scale models of landform evolution which incorporate the most recent understanding of interactions and feedbacks among geodynamics, surficial processes, and climate change (Figure 2).

Landforms develop over 10- to 100-thousand year timescales, bracketing seismic cycles and bridging the temporal gap from individual earthquakes to plate kinematics. Furthermore, they provide a convenient spatial couple between studies of surficial and crustal processes, for coherent landscape units (e.g., mountain belts) are of the order of typical continental crustal thicknesses (~10-100 km) in areal size and provide information regarding tectonic processes at that scale.

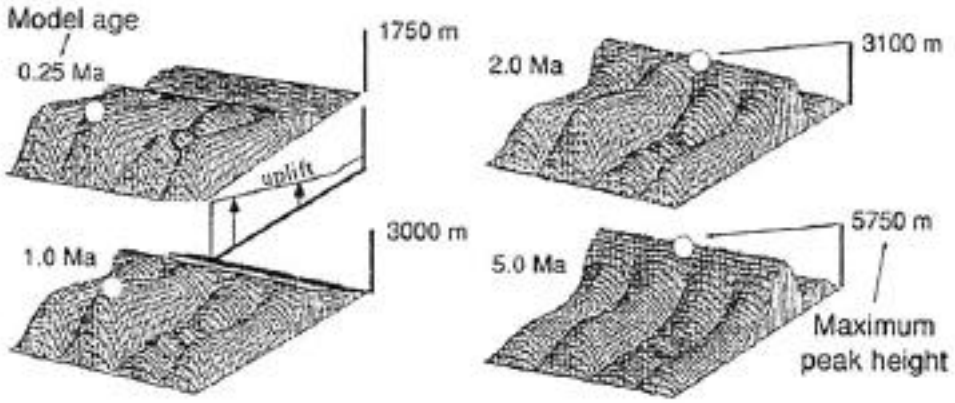

For each model age step, the position of the highest topography is shown by the open circle. Channels are dictated to have a particular shape draping between the mountain crest and the sea. The complex ridge pattern reflects the essence of that observed in the Southern Alps of New Zealand. Modified after Koons (1989).

FIGURE 2. The first two-dimensional numerical model of landscape evolution, and the first landscape model to incorporate the effects of climate. Focusing on the Southern Alps of New Zealand, Koons (1989) modeled landscape evolution in response to a plausible pattern of rock uplift, stream channel incision, and hillslope diffusion of mass that varied spatially in response to rainfall patterns. Unlike later landscape evolution models, channel positions and profiles are fixed in position and shape, respectively. This study indicated the need to consider the role of bedrock incision by streams in long-term landscape evolution. (*From* Figure 11.11, Burbank and Anderson, 2001, *after* Koons, P.O., 1989, The topographic evolution of collisional mountain belts: A numerical look at the Southern Alps, New Zealand: American Journal of Science, v. 289, p. 1041-1069.)

B. Fundamental Questions in Studies of Tectonics and Topography

Study of the interrelations between tectonics and topography is remarkably integrative, drawing upon geophysics, geomorphology, sedimentology, paleoclimatology, tectonics, and numerous other fields. The interplay of horizontal and vertical motions of crustal rocks with erosion and deposition by surface processes generates landscapes that are somewhat like palimpsests--parchments that are erased and reused over and over again, leaving behind occasional, partial residues of earlier markings. With the often complex, but frequently rich, record of tectonic and erosional forces left behind in a landscape, the following questions can be addressed.

1. How can we determine rates and styles of tectonism from landscapes?

2. How do rates of slip on individual faults compare to regional rates of deformation along plate boundaries?

3. Are similar patterns of deformation repeated during successive earthquakes on a given structure, producing landforms that reflect structural and tectonic controls?

4. How much of the cumulative deformation that generates a landform is coseismic and how much is interseismic?

5. What factors determine mega-scale differences among mountain belts, and how does climate affect topographic form?

6. Does erosion affect rates and/or styles of mountain building? Can erosion build mountains?

7. How do landscapes evolve as rates of tectonism wax and wane? I.e., do topographic forms pass through predictable stages? Do they reach "steady-state" conditions?

8. If the rate or duration of tectonic forcing changes, how does the landscape respond, and what are its response times?

C. Feedbacks between Mountain Building and Erosional Processes

One of the most obvious, and spectacular, illustrations of active tectonism is the crumpled mass of rocks that forms a mountain belt. Mountain building is associated with the addition of mass (e.g., magma) or heat, or both, to part of the Earth's crust. Crust is thickened by magma upwelling or by convergence of two plates, as in the collision zone between the Indian and Eurasian plates. As continental crust of India rams into the Eurasian plate, its is shoved underneath southern Asia. At the deformation front, the crust of both plates breaks along reverse faults, stacking imbricated sheets of rock one upon another (Figure 3).

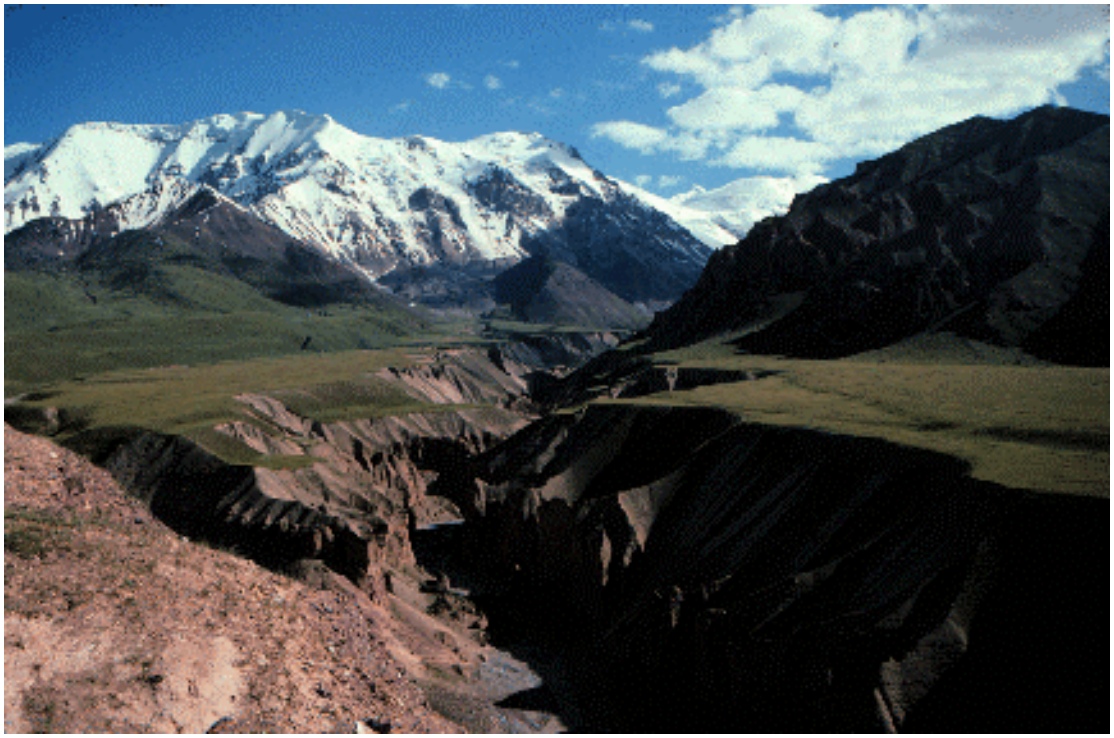

FIGURE 3. The Trans Alai Range, Kyrgyzstan, is part of the northern Pamirs, a western extension of the welt of mountains forming along the Indian-Eurasian collision zone. In this view upstream (south) along the Minjar River drainage, stacked thrust sheets are exposed at the mountain front. The top of the range consists of a thrust sheet of Paleozoic rocks overlying Cretaceous rocks (grey rocks in center field of view), which in turn are thrust over Neogene conglomerates (middle right field of view). Incision of the Minjar River in response to uplift of the hanging wall of the major south-dipping range-bounding thrust fault (Main Pamir Thrust) has produced a remarkable flight of fluvial terraces (foreground). Terraces are undeformed, suggesting that deformation is localized at the range front, 4 km behind the viewer. (*From* Arrowsmith, J.R., and Strecker, M. R., 1999, Seismotetonic range-front segmentation and mountain-belt growth in the Pamir-Alai region, Kyrgyzstan (India-Eurasia collision zone): GSAB, v. 111, no. 11, p. 1,665-1,683.)

Some of the highest uplift rates in the world, locally as much as 5-10 mm/yr, contribute towards growth of the Himalayan Mountains and elevation of the Tibetan Plateau. Rates of erosion also are some of the highest in the world, because processes of downwasting--including incision of bedrock by streams and glaciers, or the sloughing of rock mass from canyon walls by landslides--are gravity-driven. The higher and steeper the slopes of mountains and canyons, the faster the rates of downwasting.

The processes of deformation, uplift, and erosion operating in a mountain belt are so interconnected that mountains themselves can be viewed as systems regulated by numerous feedback mechanisms (c.f., Pinter and Brandon, 1997). Although movements of vast lithospheric plates ultimately create mountains, an important negative feedback between uplift and erosion controls rates of uplift and the elevation of Earth's surface. In a negative feedback, the reaction to an initial action is such that the original action is slowed and stabilized at a lower rate.

Negative feedback between the two processes of uplift and erosion works in the following way. Uplift increases the elevation of the surface of the land. If the uplift rate increases, so too does the rate of erosion, lowering the elevation of the land surface. By lowering the land elevation, erosion decreases the rate of uplift of the land surface.

Negative Feedback:

Uplift ¾> Increased Elevation ¾> Increased Erosion ¾> Decreased Elevation

If rates of uplift and erosion balance one another, a **steady-state** mountain system might result, remaining at the same general (mean) elevation and retaining a somewhat constant shape (e.g., hillslope and stream gradients) with time, even if tectonic input continues. In this manner, immense amounts of rock can be raised upward through the crust and stripped off of rising mountains. A steady-state orogen, then, is one in which rates of input and output of mass to the orogen are equivalent over a period of tens of thousands to millions of years.

Another feedback, one that is positive, links erosion to tectonism through isostasy, or crustal buoyancy. As streams incise into a rising mountain, they

remove rock mass and transport it elsewhere, typically to low basins and plains beyond the mountain belt. Removal of mass makes continental crust lighter, causing it to buoy upward to replace about 80 percent of the mass lost. This uplift results from erosion, rather than from horizontal motion of plates (Figure 4). The original action was uplift, so further uplift due to erosion is a positive feedback. The greater the rate of uplift, the greater the rate of erosion (negative feedback), and hence the greater the rate of isostatic uplift (positive feedback).

Positive Feedback:

Uplift ¾> Increased Elevation ¾> Increased Erosion ¾> Isostatic Response
(uplift)

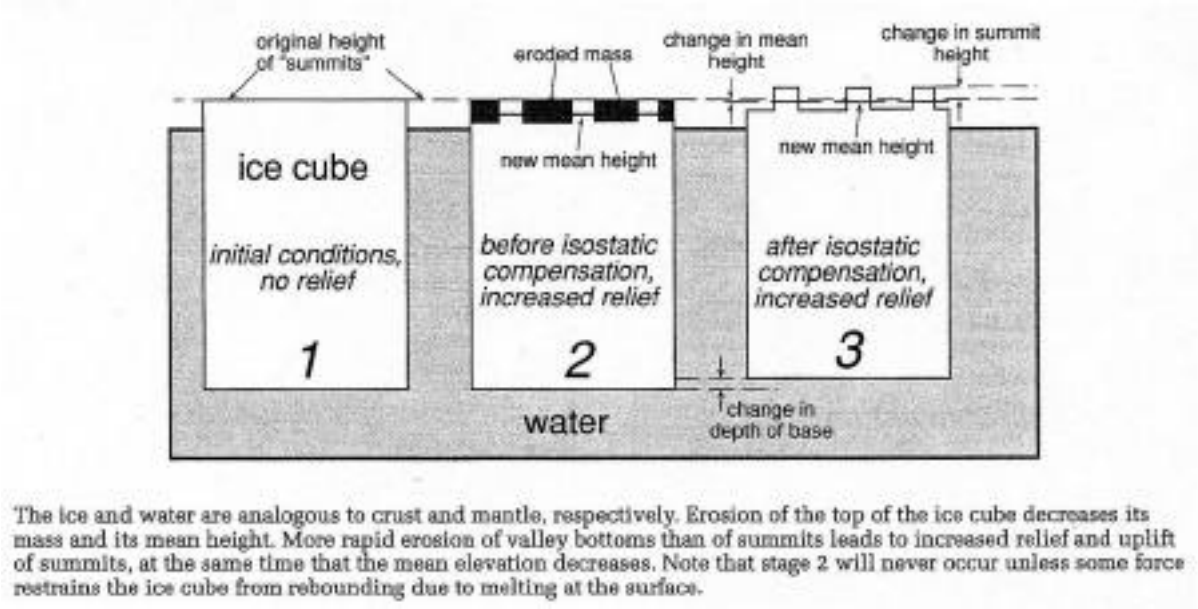

FIGURE 4. Enhanced erosion of continental crust can lead to isostatic uplift of mountain summits, as illustrated in this example of an ice cube floating in water. The ice and water are analogous to Earth's crust and mantle, respectively, with the former being less dense than the latter. Initially, the ice cube has no relief at its surface and the mean elevation of the surface floating above the water is about $1/10^{th}$ that of total ice thickness. As the top of the ice cube erodes along "canyons", the cube's mass and mean height decrease. The base of the cube rises upward as the ice compensates and achieves isostatic balance. Since erosion is more rapid along valley bottoms than at summits, relief increases and summits are uplifted even while the mean elevation decreases. (*From* Figure 1.5, Burbank and Anderson, 2001.)

An important concern of tectonics and topography in recent years has been the question of whether or not enhanced rates of erosion in Cenozoic time, perhaps in response to the onset of Ice Age glaciation, could lead to isostatic uplift and increasing relief as residual summits rise above the surrounding terrain (e.g., Molnar and England, 1990; Small and Anderson, 1995). Conversely, others have suggested that accelerated uplift during the Cenozoic Era might have led to global cooling and the onset of glaciation. This dilemma has been referred to as the chicken or egg problem, as it is difficult to determine which process must have come before the other.

'Chicken':

Ice Age ¾> Increased Erosion ("erosional buzzsaw") ¾> Isostatic Response

'Egg':

Uplift ¾> Increased Elevation ¾> Glaciers/Global Cooling

In the long-term, as rates of tectonic uplift decrease in a mountain belt, erosion begins to dominate. Erosionally-driven isostatic uplift continues, but will be insufficient to prop up the mountains, so the land surface gradually lowers. Ancient mountain belts, such as the Appalachians or Caledonians, are much lower than younger and still active mountains, such as the Andes or Himalayas.

Like the Himalaya , the modern world's largest topographic anomaly, the Appalachian Mountains formed as the result of continental collision--the same collision that created Pangaea about 350 My ago. While still actively growing, their average elevation is estimated to have been some 3 to 5 km. The difference between the two mountain systems is their age. Uplift of the Appalachians culminated about 250 to 350 million years ago, whereas the Himalayas began forming about 50 million years ago. Still growing through tectonic activity, the Himalayas are thought to be the largest mass of rock at such high altitudes in the past billion years of Earth history (c.f., Pinter and Brandon, 1997). Many Himalayan peaks, including Mount Everest, exceed 8 km, and average elevation of crust above the geoid is 5 km (Figure 5).

Erosion and erosionally-driven isostatic uplift, in contrast, dominate the Appalachians. About 4 to 8 km of material might have been stripped from the Appalachian Mountains during the past 270 million years (see Pinter and Brandon, 1997).

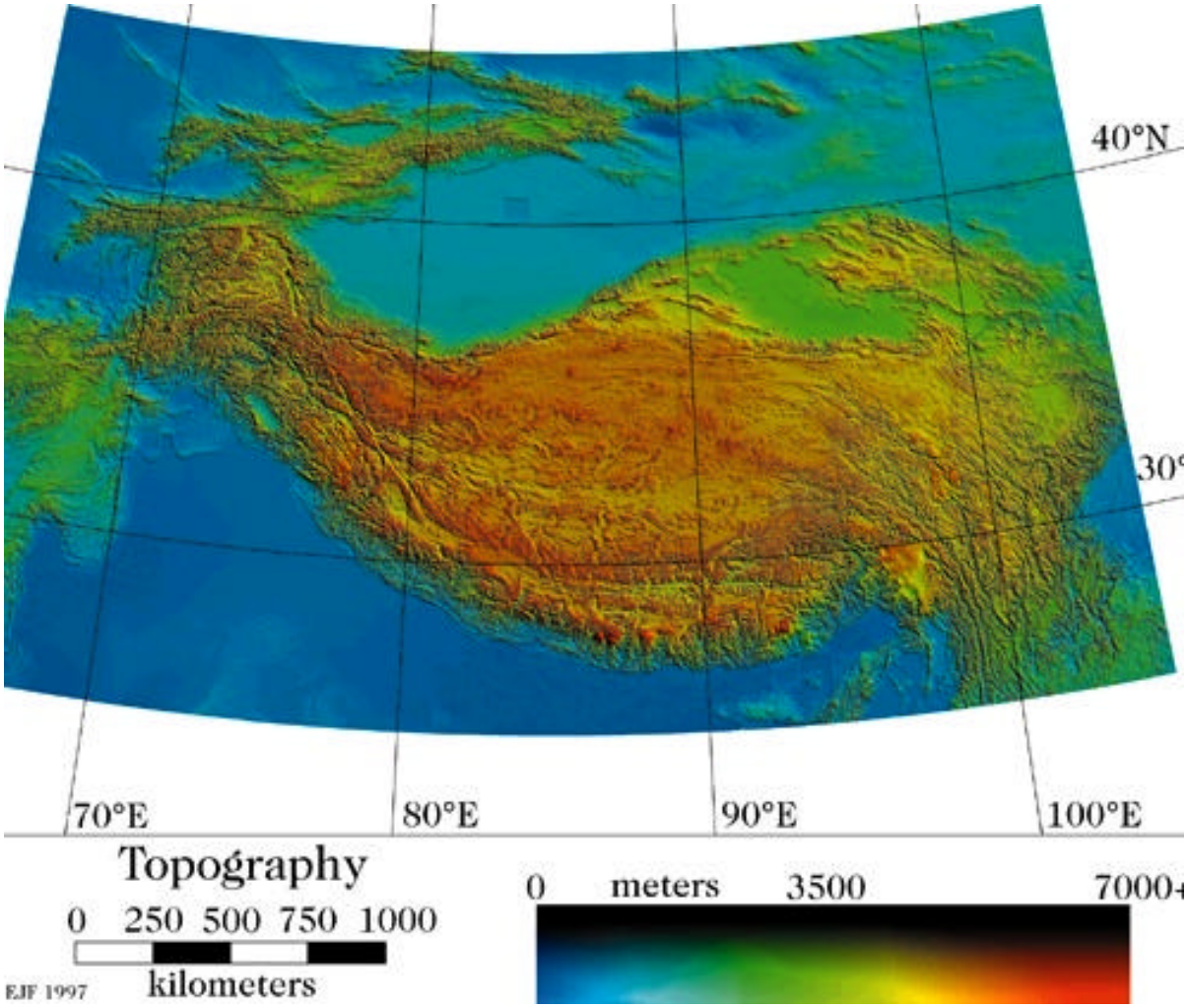

FIGURE 5. Still growing since collision began about 40-50 My ago, the Himalaya and adjacent Tibetan Plateau to the north represent possibly the largest mass of mountains that has existed on Earth in the past billion years. Deep bedrock erosion along canyons (both fluvial and glacial) in the Himalaya, and resulting isostatic compensation, might explain the contrast between the altitude of the Himalayan peaks and the low-relief Tibetan Plateau (Image from Eric Fielding; see Fielding, E. J., Isacks, B. L., Barazangi, M., and Duncan, C., 1994, How flat is Tibet? Geology, v. 22, p. 163-167.)

Activity: Tectonics and Topography Earthscape Images

In the Summer of 2001, the workshop convenors sent a request to members of the Tectonics and Topography community for digital images that represent key study areas throughout the world. The images were compiled by Mike Rahnis and are available on the CD that accompanies this workshop manual. Each set of images contains detailed captions and references pertinent to the work done in that area. In addition, the images can be viewed at both low and high resolution (TIFF). In any future reference to these images, please acknowledge the names of the individuals below. Individual images are copyrighted by their submitters. If you use images as compiled on the CD, please acknowledge Rahnis and Merritts, 2001.

To access the images, open the folder titled "Gallery", then double-click on the "index.html" file. From there, browse through the different contributions, as listed below.

Indo-Australian-Eurasian Plate Convergence/Collision

Thrust faulting--northern Pamir Mountains, Kyrgyzstan
(Ramon Arrowsmith and Manifred Strecker)

Strike-slip faulting--Altyn Tagh fault, Tibetan Plateau
(Ramon Arrowsmith, Z. Washburn, et al)

Folding and faulting, Tien Shan, Kyrgyzstan (Doug Burbank)

Island emergence in a collision zone—Taiwan (Rudy Slingerland)

Cocos Plate-Caribbean Plate Convergence/Subduction

Uplift above an aseismic ridge on a subducting plate--Costa Rica
(Tom Gardner)

Pacific-North American Plate Transform Motion

Transpression along bends in strike-slip faults--San Andreas fault system, Santa Cruz marine terraces, California (Bob Anderson)

Rapid uplift and bedrock incision at the northern termination of the San Andreas fault system, Mendocino triple junction
(Dorothy Merritts and Noah Snyder)

Juan de Fuca-North American Plate Convergence/Subduction

Jaun de Fuca-North American Plate Convergence/Subduction (Frank Pazzaglia)

Rates of bedrock erosion/incision

Measuring rates of bedrock incision--Valley of Ten Thousand Smokes, Alaska
(Kelin Whipple and Noah Snyder)

See also: Pazzaglia (above) and Merritts and Snyder (above)

II. Recent Advances in Studies of Tectonics and Topography

In recent decades, a number of new technologies and advances have enabled researchers in tectonics and topography to use more rigorous means of analysis in order to resolve long-standing questions. Here, we list some of the most important of these technologies and advances.

A. Synopsis of Recent Advances

- **Chronologic techniques**--New means of dating rocks, deposits, and bedrock surfaces provide quantitative controls on rates of deformation and erosion (see Table 1). Until the 1970s-1980s, geomorphologists relied mostly upon

TABLE 1. Absolute Dating Methods (modified from Burbank and Anderson, 2001)

Method	Useful Dating Range	Suitable Materials	Partial list of Relevant References
Radioisotopic			
^{14}C	35-40 ka	Wood, shell	Libby, 1955; Stuiver, 1970
U/Th series	10-350 ka	Carbonate (coral, speleothems)	Ku, 1976; Edwards et al, 1987
Thermoluminescence	30-300 ka	Quartz silt	Berger, 1988
Optically stimulated luminescence	0-300 ka	Quartz silt	Aitken, 1998
Cosmogenic			
In situ ^{10}Be, ^{26}Al	3-4 Ma	Quartz	Lal, 1988; Nishiizumi, 1991
He, Ne	Unlimited	Olivine, quartz	Cerling and Craig, 1994
^{36}Cl	0-4 Ma		Phillips et al, 1986
Paleomagnetic			
Reversals	>700 ka	Fine sediments, volcanic flows	Cox et al, 1964
Secular variations	070 ka	Fine sediments	Creer, 1962; Lund, 1996
Biological			
Dendrochronology	10 ka with local master chronology	Wood	Fritts, 1976; Jacoby et al, 1988; Yamaguchi and Hoblitt, 1995

relative dating methods that included 1) degree of boulder weathering (quantified sometimes with statistical analyses of many boulders and/or measurement of propagation speed of seismic waves through clasts; 2) development of weathering rinds (quantified with statistical analyses of many clasts); 3) degree of soil development on a depositional surface; 4) accumulation of calcium carbonate coatings on clasts or in soil matrices; and 4) lichen diameters on bedrock or clast surfaces.

- **Paleoclimatology**--In large part as a result of advances in chronologic techniques, the record of past climate change is much better calibrated than ever before. Magnitudes and rates of change during the late Quaternary period, in particular, have been gleaned from studies of isotopes in air bubbles taken from cores of ice and in organic-rich sediments taken from deep-sea sediment cores.

- **Paleoseismology**--Again due to advances in geochronology, the increasingly detailed record of past earthquakes provides a foundation for examining the behavior of faults and their relation to adjacent landforms (c.f., Merritts, 1996; Prentice et al, 1999; Merritts et al, 2000).

- **Geodesy**--New geodetic tools enable measurements of changes in positions of specific points on Earth's surface and in spatial patterns of deformation resulting from earthquakes.

- **Digital topographic databases**--The topography of Earth's continental surfaces is now known at extremely high resolution and accuracy, and widely available in digital form. Combined with high-speed computers and remotely sensed imaging techniques (e.g., radar or thematic mapping imagery), digital topographic data enable relatively rapid studies of landforms at a variety of scales, from local to global (Figure 6).

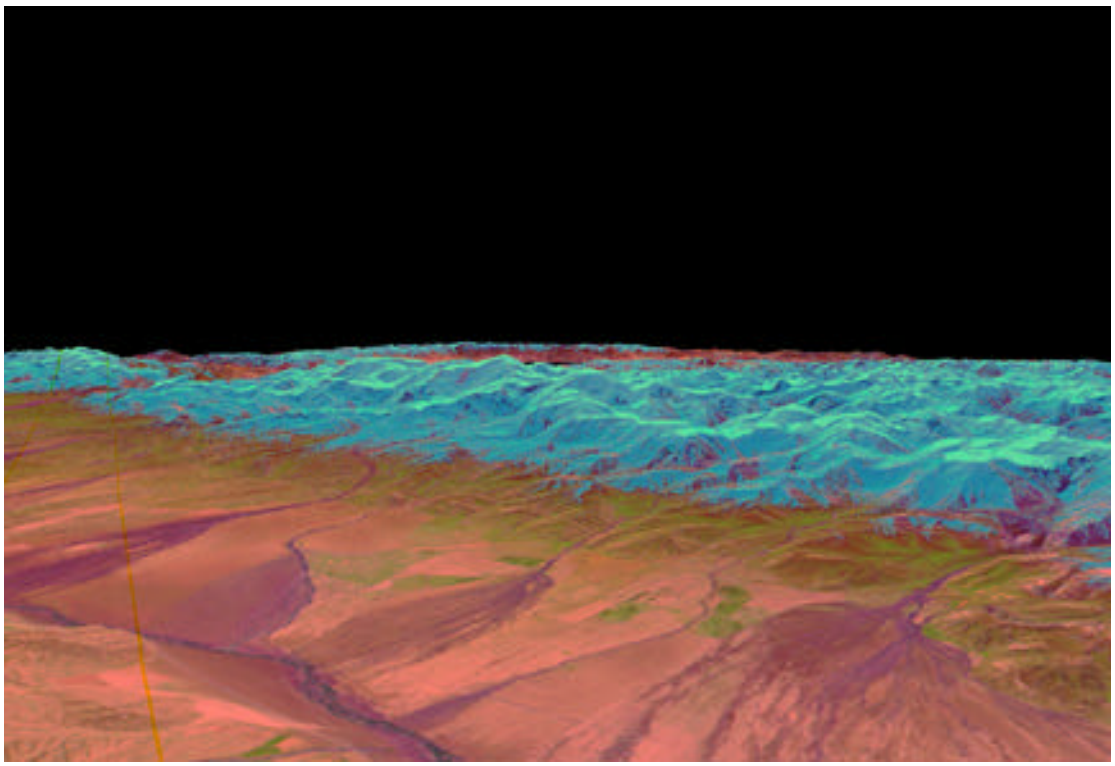

FIGURE 6. In this perspective view to the southeast of the Trans Alai Mountains in central Asia, Landsat Thematic Mapper images are draped on a digital elevation model. The digital topography is from the GTOPO30 1-km data set. The low-relief surface in the foreground is the Alai Valley. The range front is bounded by the active Main Pamir thrust. (*From* McManus, Sean, 1998, Digital elevation model analysis applied to active tectonic study in central Asia: M.S. thesis, Arizona State University, 86 p.)

· **Numerical modeling**--With the advent of computer technologies, it is possible to model tectonic and surface processes and resultant landforms (i.e., model output) in order to explore interactions among different variables, to determine sensitivities of different processes, or to estimate the response times of various processes to external change (Figures 7 and 8).

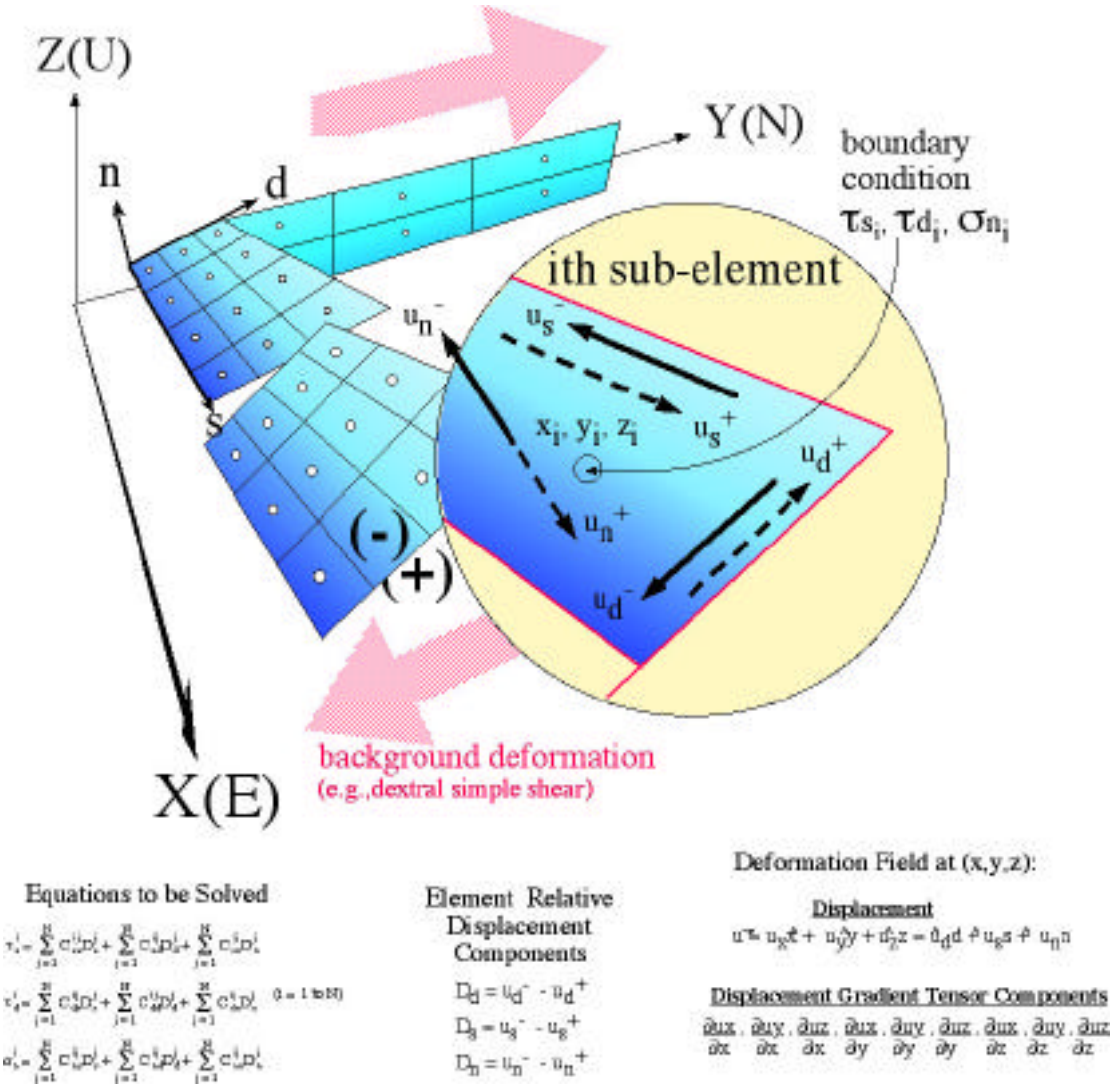

FIGURE 7. Cross-talk among faults in complicated fault systems can be explored with 3DDEF (3-D deformation), a half-space boundary-element code in which deformation is driven by far-field shear stresses, resulting in slip along fault planes. Fault surfaces (shaded planes) are subdivided into sub-elements with boundary conditions specified at center (white dots). Uniform background simple-shear displacement field can be specified to drive fault displacements. Deformation field can be calculated at any observation point once relative displacement components on each sub-element are known. (*From* Gomberg and Ellis, 1994.)

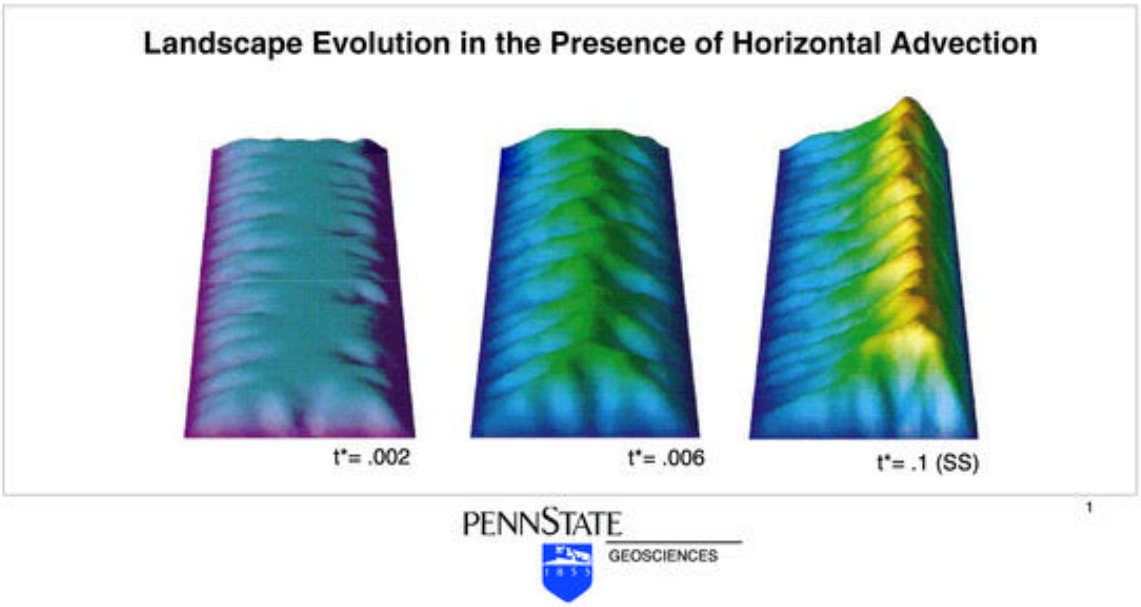

FIGURE 8. In contrast to the 3DDEF modeling shown in Figure 7, this model output represents simulation modeling used to explore the relations among rock uplift, climatic factors (e.g., wind direction, precipitation amounts), and erosion. This model of based on studies in Taiwan, from the work of Willett, Slingerland, and Hovius (2001).

B. Mapping Global Topography and Deformation with Airborne and Space-Based Measurements

All tectonic plates are in motion, so the ideal way to determine the absolute velocity of any given part of a plate at Earth's surface is to fix an object to the plate and then to track its motion from an observation point in outer space. Alfred Wegener proposed such a test for his ideas on continental drift in 1929, making the following prediction: "I have no doubt that in the not too distant future we will be successful in making a precise measurement of the drift of North America relative to Europe".

Decades ahead of his time, Wegener was correct, but didn't live to see his prediction borne true. Lacking such direct confirmation of the mobility of tectonic plates, it was to be another 50 years until geologic and seismologic evidence convinced the scientific community of the reality of plate tectonic motions. Using *space geodesy*, the precise measurement of the shape and motion of the Earth's surface from space-based instrumentation, we have now fulfilled Wegener's dream of directly measuring the drift of the Earth's tectonic plates.

Geodesy is the science concerned with the measurement of the size, shape and motion of the Earth and its surface. Space geodesy, and in particular the Global Positioning System (GPS) and Interferometric Synthetic Aperture Radar (INSAR) measurements are about to revolutionize much of the earth sciences beyond measuring plate motions. We can also measure the deformation patterns in between, during, and following individual earthquakes along a crustal fault in great detail. Studies of the distribution of deformation along a plate boundary zone can identify regions of particularly active deformation and help in earthquake hazard evaluations. Geodetic studies help elucidate the complex tectonic processes that shape the surface of the Earth. Even though most crustal deformation occurs along plate boundaries, geodetic studies of the North American mid-continent show some evidence for localized slow intra-plate deformation. Space geodesy and remote sensing may turn out to be the new rock hammer aiding the 21st century field geologists and geophysicists in their investigations of the dynamic Earth.

1. Global Positioning System

Until about 15 years ago, precise geodetic measurements relied on terrestrial methods of which triangulation, laser ranging and spirit leveling were the most commonly used. Surveyors repeatedly measured angles, distances, or elevation differences between benchmarks set in the ground. These techniques allowed the development of precisely surveyed maps and the investigation of local deformation associated with earthquakes or volcanic eruptions that displaced nearby benchmarks. Space geodesy dates back to at least 230 BC, when Eratosthenes found the Earth's size from observations of the sun's position at different sites. Only 2210 years later, we utilized the difference in the time when radio signals from distant quasars arrive at radio telescopes to determine the position and motions of those telescopes and the tectonic plates on which they reside at a few mm precision, a technique called Very Long Baseline Interferometry (VLBI).

Radio telescopes are expensive and somewhat unwieldy, therefore it was the establishment of the NAVSTAR satellite constellation and the Global Positioning System (GPS) that brought space geodesy to the common geophysicist and geologist. More than two dozen satellites orbit the Earth at all times, each containing a highly precise atomic clock and each transmitting radio signals. On the ground, a receiver compares the amount of time it takes radio waves to reach its station from multiple satellites (typically four or more) scattered above it in the sky. Differences in the travel times provide an estimate of the receiver's horizontal location to within 1 cm. By tracking the position of receivers mounted on different parts of plates over a period of years, researchers now are able to determine absolute velocities of plates all over the world. The short-term rates measured over a period of years are remarkably similar to the longer-term rates over millions of years that are determined from sea-floor spreading and hot-spot tracking.

Continuously operating GPS receiver networks are slowly covering many regions of seismic or volcanic hazards to measure in great detail the intricate motions associated with the earthquake cycle and active volcanoes.

2. InSAR (Interferometric Synthetic Aperture Radar)

[Note: PDF file of Bürgmann, Roland, Paul A. Rosen, and Eric J. Fielding, Synthetic Aperture Radar Interferometry to Measure Earth's Surface Topography and its Deformation, Annu. Rev. Earth Planet. Sci. 2000. 28:169-209, accompanies this manual. See CD in back pocket.]

Synthetic Aperture Radar (SAR) interferometry is the latest addition to the space-geodetic arsenal of earth scientists, as it allows for precise mapping of topography, surface properties and deformation completely hands off. This latest revolution in crustal deformation studies made its spectacular entry in 1993. Using interferometric images of the European Remote Sensing (ERS-1) satellite radar data collected before and after the 1992 Landers earthquake, scientists were able to image the deformation surrounding the rupture in astounding detail. All that is needed to measure crustal deformation at cm resolution is a couple of radar images from earth orbiting space crafts. To accomplish this astonishing feat, it is necessary to interfere the phase information of reflected radio signals (echo) from observations taken several weeks or months apart. If the reflecting area has changed its relative position, a phase shift will occur that is revealed in the interferogram.

Obviously it is necessary to carefully correct for the effects of the difference in the orbital tracks when the two images were taken and to remove the effects of varying topography. Any change in surface characteristics such as vegetation growth causes a loss of coherence and it is not possible to interfere the phase data. An additional, potentially large error source comes from the differential signal delay in the Earth's atmosphere. In the resulting interferogram each fringe corresponds to one cycle of about one inch of motion away from or towards the ERS-1 satellite (half the 56-mm wavelength of the SAR). The ultimate precision of SAR interferometry is at the millimeter level, with dense spatial sampling of 20-80 m per pixel.

If no deformation occurred between the two radar images used to construct an interferogram, the range change observed is mostly due to the effects of topography viewed from slightly different perspectives. It is thus possible to produce a digital elevation model (DEM) of meter scale accuracy from these interferograms. Airborne systems (such as the NASA AirSAR program) rely on a dual-antenna system mounted on a GPS navigated plane. The Shuttle Radar Topography Mission (SRTM) was dedicated to the production of a

precise global DEM and utilized a receiving antenna located on a boom extended 60 m from the primary antenna on the shuttle. Most systems rely on single-antenna satellites requiring that the spacecraft closely repeat the initial orbit to produce a second SAR image for interferometry. The tandem mission of the European Space Agency (ESA) ERS-1 and ERS-2 spacecrafts had the two satellites follow each other along the same orbit so that a common area was imaged at 1-day time separation to allow for the generation of topographic maps.

III. Crustal Deformation and Landscape Generation

A. Fault Scarps and Fault Slip: Morphological Features and Crustal Movements

An example of a morphological feature produced by crustal movements is a fault scarp. Until 1891 most scholars believed that shaking during earthquakes caused the ground to crack and form both faults and associated topographic scarps. In that year a large earthquake in Japan formed a scarp up to 6 m high and 70 to 80 km long, offsetting many physical features as much as 5.5 m in both horizontal and vertical directions. In direct contrast to common thinking of the time, geologist Bunjiro Koto proposed that offset along the fault had caused the earthquake and the scarp, not the other way round.

In 1906 Koto's idea gained wide acceptance when a large earthquake that destroyed San Francisco was linked directly to slip along a known fault—the San Andreas (Figure 9). Before the earthquake, geologists had noted that rock types on each side of the fault do not match. Geologists who flocked to the area after the earthquake discovered up to 8 m of horizontal offset of rocks, fences, hillsides, and even walls of buildings along the length of the fault, over a distance of nearly 200 km. It now is well documented that most earthquakes are the result of plate motions that strain the rocks along a fault plane until they slip. The resultant shaking is due to the release of energy stored in rocks on each side of a fault before they snap and slip past one another.

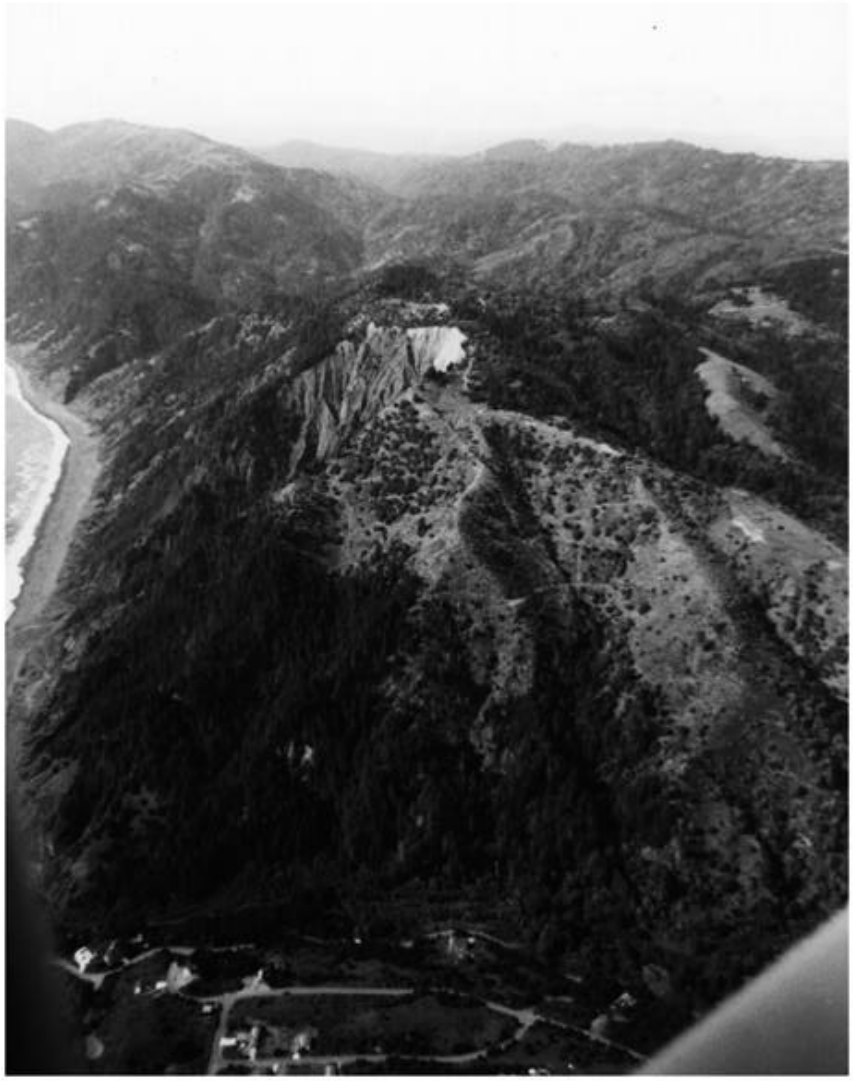

FIGURE 9. Right-lateral transform motion between the Pacific and North American plates produces slip along the San Andreas fault, coastal California. View to north of Telegraph Hill (T), at the northern termination of the San Andreas fault system. Note prominent east-facing scarp indicated by long, white arrows. Scarp diverges into two traces, marked by short, white arrows, near top of hill. Sense of motion on the main trace (westernmost scarp) is oblique, with both right-lateral and reverse (up to the west) motion. Kaluna Cliff (KC) is in middle ground. Prominent notch (N) along skyline marks northernmost feature identified as possibly related to Quaternary fault activity. Low-sun-angle oblique aerial view taken in June 1995 by photographer Cheryl Stolzfus Shenk. (*From* Prentice, Carol S., Merritts, Dorothy J., Beutner, Edward C., Bodin, Paul, Schill, Allison, and Muller, Jordan R., 1999, Northern San Andreas fault near Shelter Cove, California: GSAB, v. 111, no. 4, p. 512-523.)

For the past several decades, geologists have mapped and surveyed fault scarps on many continents, sometimes just after large earthquakes. Such studies have contributed much to our understanding of seismotectonics. In addition, they have laid the modern foundations for paleoseismology and tectonic geomorphology.

Along the northern margin of the Tibetan Plateau, for example, Z. Washburn, J. R. Arrowsmith, and others used a combination of detailed mapping, trench excavations, and radiometric dating to identify segment boundaries, slip rates, and recurrence intervals along the predominantly left-lateral Altyn Tagh fault (Figures 10 and 11; Washburn et al, in press). Slip rates acquired from fault scarp analysis can be compared to rates of relative motion between plates, leading to greater understanding of how systems of faults accommodate plate motion. The Altyn Tagh, for instance, is one manifestation of the regional accommodation of convergence between the Indian and Eurasian plates.

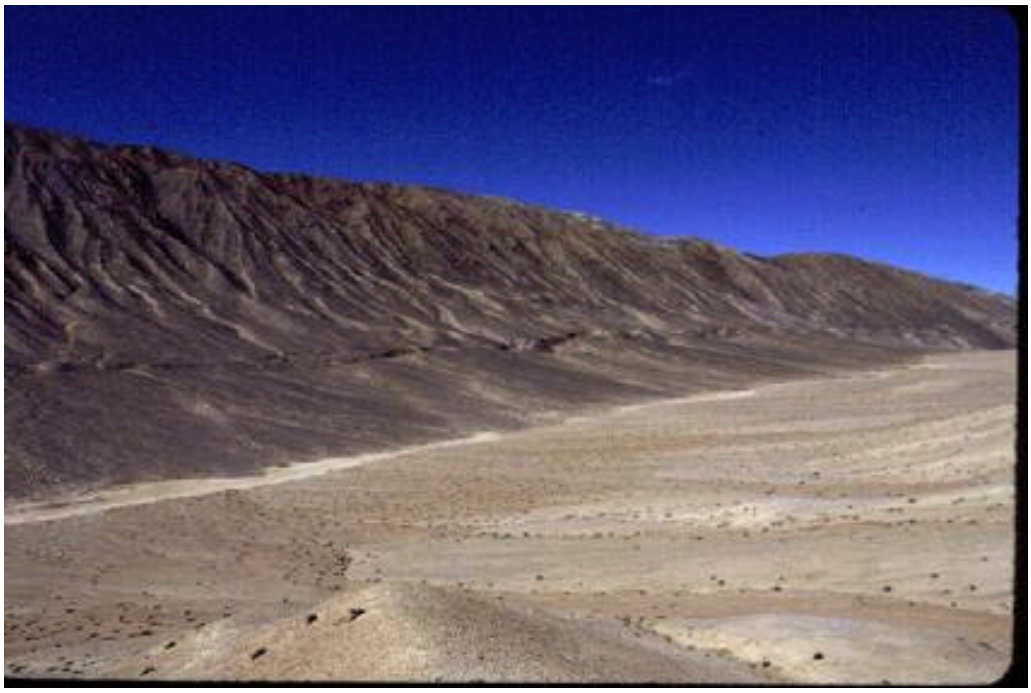

FIGURE 10: This southwest view of the GoBiLing rupture zone illustrates some of the best-preserved and largest apparent single event offsets along the central Altyn Tagh fault, at an elevation of about 3800 m. The area also shows interaction features (pop-up structures) along discontinuous, en echelon rupture traces and larger offsets. (*From* Washburn, A., et al,, Recent earthquake geology of the central Altyn Tagh Fault, China: Geology, in press, 2001.)

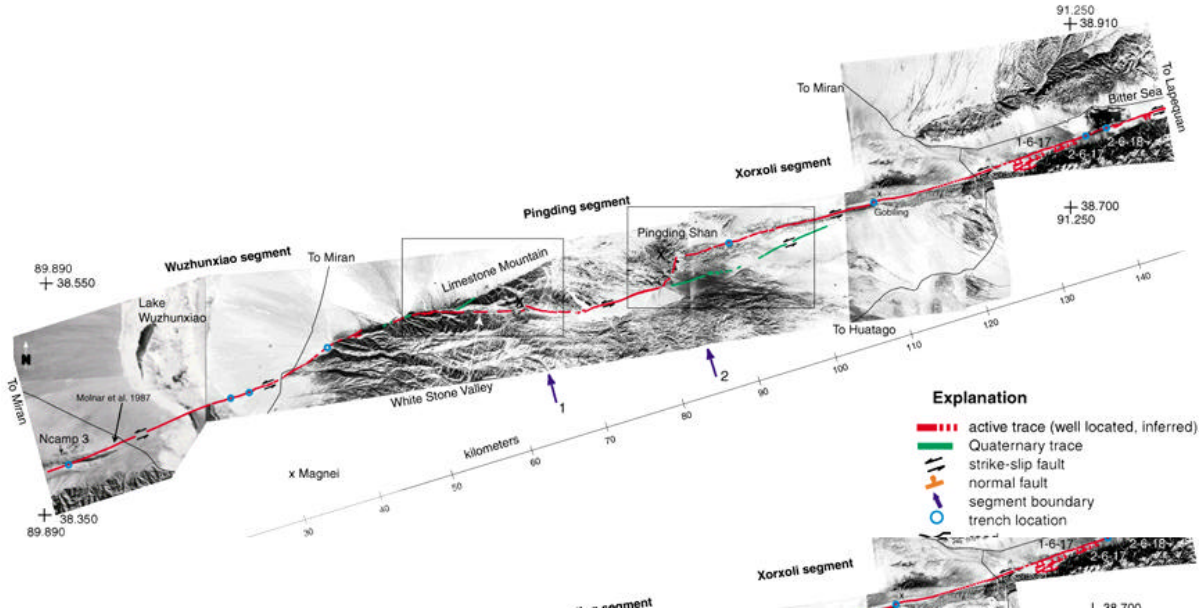

FIGURE 11: Portion of detailed mapping along the Altyn Tagh by Washburn et al (in press) revealed discontinuous, en echelon rupture traces and deformation structures, including pressure ridges. (*From* Washburn, A., Arrowsmith, J. R., Forman, S. L., Cowgill, E., Wang, X. F., Zhang, Y. Q., and Chen, Z. L., Recent earthquake geology of the central Altyn Tagh Fault, China: Geology, in press, 2001.)

Deducing rates of deformation from tectonically-generated landforms requires age control (Figure 12). Numerous advances in the dating of surficial deposits have contributed to studies of paleoseismology and tectonic geomorphology. Most landforms of interest in active tectonics are Quaternary in age, so radiocarbon dating--with a dating span of about 40,000 yrs--has been of limited value. Furthermore, organic matter typically is rare in alluvial, glacial, or colluvial deposits in semi-arid and arid regions. More recent advances in a variety of other techniques, including cosmogenic isotope and thermoluminescence dating, have contributed substantially to estimating the ages of deposits offset along active faults, and hence in determining rates of deformation.

FIGURE 12. Syrinadjar fault zone and scarp, central setion of Main Pamir Thrust, Kyrgyzstan. This thrust fault is another manifestation of convergence between the Indian and Eurasion plates. View is east-southeast across the Syrindajar River. The 18-m high fault scarp cuts an early to middle Holocene terrace surface, and downcutting by the Syrindajar River has exposed the fault beneath the scarp. The scarp is less than 6 ka in age and the thrust fault dips 30° south, yielding a slip rate of >6 mm/yr. Vehicle and tents at base of scarp, and person in channel bottom in foreground, provide scale. (*From* Arrowsmith, J.R., and Strecker, M. R., 1999, Seismotetonic range-front segmentation and mountain-belt growth in the Pamir-Alai region, Kyrgyzstan (India-Eurasia collision zone): GSAB, v. 111, no. 11, p. 1,665-1,683.)

B. Uplift and Mountain-Building along a Strike-Slip Fault: Case Study of the Northern Termination of the San Andreas Fault

Geomorphic characteristics and geologic relations at the northern end of the San Andreas fault (SAF), in the Mendocino triple junction (MTJ) region, reveal a complex pattern of active deformation, with increasing uplift rates northward along the tip of the fault. Our earlier work (Prentice et al., 1999) established that an active trace of the SAF returns to shore at Point Delgada, ~25 km south of the triple junction (see Figure 9). This trace strikes about N10-15W and can be clearly mapped for at least 3 km. Along the same strike, a possible 10-km inland continuation of the fault to the north of Point Delgada is less well-defined. An onshore location is contrary to the commonly mapped, hypothetical offshore SAF as it approaches the MTJ. If the onshore trace of the SAF is also the long-term bedrock plate-boundary fault, then rocks exposed in the King Range to the west of the SAF are part of the Pacific plate, and the triple junction itself exists onshore. Resolving this possibility requires knowledge of the nature and duration of tectonism along the northernmost SAF.

Merritts et al (2000) proposed that the SAF changes in character as the fault approaches its initiation point at the MTJ. King and Nabelek (1985) argued from geometrical analyses of finite motion on two strike-slip faults that faulting in a third direction is created where the two meet at an angle. Furthermore, additional faulting near the juncture point will be complex and multidirectional. For each of the major strike-slip faults, displacement must approach zero at their junction, producing a slip deficit and high strain around the tip of each fault. In order to accommodate finite deformation, a system of subsidiary faults—a fractal set—forms. Corresponding increases in displacement occur on these off-fault structures in a crushed region surrounding the junction point, so that constant total displacement is maintained. This crushed region is a process zone, an area of intense faulting and deformation at the highly-strained end of a fault where it joins another fault. The rugged landmass undergoing rapid uplift to the west of the onshore termination of the SAF, the King Range, might represent such a crushed region. If so, it should become increasingly difficult to locate an active trace of the SAF within this region, yet correspondingly easier to identify evidence of distributed deformation along multidirectional, subsidiary faults.

Merritts (1996) and Merritts et al (2000) surveyed and radiometrically dated deformed Holocene and late Pleistocene marine terrace platforms and alluvial deposits that occur on both the western and eastern sides of the SAF as it approaches the MTJ. The geometry of the wave-cut platform(s) at Point Delgada indicates that it does not dip gently seaward (westward), as do all wave-cut platforms at the time of formation; instead, it has been rotated eastward, so that it tilts into the plane of the SAF. Merritts et al (2000) surveyed about 330 points along the fringe of bedrock platform rimming the point, then plotted the data as a mesh grid and performed a first-order trend surface analysis. The direction of maximum slope for the first-order surface is S22E. The tilt of the platform is 3.8 m/km to the southeast along a S22E direction. Rotation of the wave-cut platform from a west-dipping, or seaward, direction to an east-dipping direction is consistent with multiple lines of evidence of up-to-the-west motion for the SAF at Point Delgada. In essence, the wave-cut surface reveals a large-amplitude drag fold, similar to smaller-amplitude drag folds that we examined in the rock fabric immediately west of the fault plane. The direction of tilt is similar to a passive marker, in that its counterclockwise rotation with respect to the trend of the SAF (N10-15W) is consistent with dextral shear.

Wave-cut platforms and their overlying marine and alluvial sediments have been offset right-laterally along the SAF as well as tilted vertically. The majority of the alluvial sediments consist of debris-flow gravel deposited in thick beds within several abandoned alluvial fans that lie stratigraphically above the thin veneer of beach gravel on the wave-cut platforms. We propose that the alluvial fan gravel between Shelter Cove and Point Delgada has been warped and translated laterally from its source at Dead Man's Gulch, which is southeast of Shelter Cove today. The fan was abandoned sometime after 13,180 ±170 yr BP (radiocarbon date from uppermost alluvium). East of the SAF, an abandoned fluvial terrace at the mouth of Dead Man's creek is cut into Franciscan argillite about 20 m above the beach, marking the apex of the now detached fan to the west of the SAF.

Determining a precise amount of right-lateral translation is difficult because distinctive piercing points do not exist. However, by reconstructing the shape of the abandoned fan, taking into account the northwest paleocurrent direction of its gravels, and aligning the fan with the fluvial terrace at Dead Man's Gulch, we estimate ~270±30 m of offset. Using the age of 13,180 ±170

yr BP from the fan's uppermost strata as a maximum possible age for abandonment yields an approximate long-term slip rate across the SAF of 21±2 mm/yr, similar to slip rates estimated farther south at Point Arena (25±3 mm/yr).

Merritts et al (2000) use a three-dimensional boundary-element algorithm that accounts for interaction among fault segments to explore uplift patterns along the coast to the west of the SAF. The boundary-element technique predicts reasonable deformation fields (vertical and horizontal) that can be compared with actual field data, such as surface uplift rates obtained from emergent marine platforms. The goal of the modeling is to determine whether or not an onshore location for the SAF is sufficient to account for the rapid increase in uplift that occurs northward of Point Delgada, and the south-eastward tilt of the platform into the SAF plane at Point Delgada. A model with an onshore SAF that tapers in depth to the north and terminates near Saddle Mountain results in a deformation field with many similarities to the observed deformation pattern. The model-generated uplift rate at Point Delgada is 0.1 m/ky, and the coast is tilted N80E at a rate of 0.01 m/km/ky. To the north, the uplift rate increases to a maximum value of 1.3 m/ky at Big Flat. These values agree well with those obtained from analysis of deformed Pleistocene and Holocene marine terrace surfaces (Merritts, 1996).

Exercise: Reconstructing Sea-level Change from Emergent Marine Terraces

Glacially controlled worldwide (eustatic) sea-level fluctuations have occurred over time periods of 10^4-10^5 yrs (glacial/interglacial cycles). At time scales of 10^3-10^4 yrs, the deglacial hemicycle of the last ice age (the most recent 10,000 yr, or Holocene Epoch) is well constrained.

Glacial-cycle sea level changes are obtained from two sources:

1) emergent (uplifted) coral reef terraces on tropical coasts;
2) deviations from a standard of the O^{18}/O^{16} ratios in foraminiferal tests from deep-sea cores.

In this exercise, we use actual data of type 1 (coral reef terraces) to reconstruct a sea-level curve for the past 140,000 yrs. Uranium-thorium series dates provide age control. The procedure is much the same as that used by John Chappell, Art Bloom, and others to reconstruct a paleo-sea-level curve from their studies of emergent coral reef terraces in New Guinea in the 1970s to 1980s.

You will construct a eustatic sea-level curve from known ages and present heights of individual terraces at six survey transects in New Guinea (see Table 1). Uplift rates vary nearly an order of magnitude along the coast of New Guinea's Huon Peninsula. As a result, the number and altitudes of terraces vary among the transects.

In order to reconstruct a eustatic sea-level curve, you need to determine an uplift rate for each transect before you can estimate the initial level of each coral reef terrace when it was active (i.e., its altitude of formation). Like Chappell (1974) and Bloom et al (1974), you will need to make two assumptions:

1) Uplift rates have been constant at each transect over the time period of consideration.
2) The last major interglacial highstand, which occurred ~124,000 yrs ago, had an altitude of formation of +6m. This assumption is based on the modern altitude of the 124,000 yr marine terrace at locations thought to be tectonically stable, including the main island of Hawaii.

Table 1. Measure of Reef-Crest Elevations (in meters) for Six Transects Along the Huon Penninsula, Papua New Guinea

		Transects					
Terrace	Age (ka)	Kanzarua	Blucher	Kwambu	Nama	Sambero	Kambin
VIIb	124	330	280	215	160	150	120
VI	105	250	215	160	115	110	93
V	82	190	155	117	90	80	60
IV	60	125	--	70	48	--	28
IIIa	50-40	90	65	42	--	--	--
IIIb	40	70	41	28	10	10	--
II	28	30	18	7	--	--	--
I	6	15	10	6	5	5	2.5

(From Bloom and Yonekura, 1985, Coastal terraces generated by sea-level change and tectonic uplift: in Models in Geomorphology, M. J. Woldenberg, ed., Allen and Unwin, Winchester, Mass., pp. 139-154; Table 6.1).

ANALYSIS

1. DETERMINE THE UPLIFT RATE FOR EACH TRANSECT.

		Transects					
		Kanzarua	Blucher	Kwambu	Nama	Sambero	Kambin
UPLIFT RATE	m/ky	2.61					

2. DETERMINE THE ALTITUDES OF FORMATION (m) OF EACH TERRACE.

				Transects					Standard
Terrace	Age (ka)	Kanzarua	Blucher	Kwambu	Nama	Sambero	Kambin	Mean Alt, m	Dev, m
VIIb	124								
VI	105								
V	82								
IV	60								
IIIa	46								
IIIb	40								
II	28								
I	6								

3. CONSTRUCT A SEA-LEVEL CURVE.

Plot time on the x-axis (0 on left; 150 ky on the right) and altitude on the y-axis. Save space along the left margin (about 2 inches) to plot the modern altitudes of each terrace at the Kanzarua and Kambin transects. Locate the positions of sea level highstands. Draw a line from the 124-ky highstand to the terrace altitude of that age. What is the slope of this line (literally and conceptually)?

4. DISCUSSION

Why does the 28-ky marine terrace only occur on 3 of the 6 transects?

What minimum uplift rate is required to preserve the 40-ky marine terrace at any given transect?

If a sea level high stand occurred at 92 ky and reached an altitude of -18 m, at what altitude would you expect to find a terrace of this age at the Kanzarua transect?

IV. Numerical Modeling of Landscape Evolution

D. Introduction to Numerical Modeling and MATLAB

1. MATLAB Tutorial—data analysis and plotting (see PDF file on CD that accompanies manual)

2. Gridding and trend-surface analysis of deformed wave-cut platforms along the San Andreas fault (see PDF file on CD that accompanies manual)

E. Landscape Evolution: Tectonic Uplift, Sea-level Change, and Marine Terrace Generation (MATLAB finite-difference of R. S. Anderson—see below)

(see MATLAB files on CD that accompanies manual)

F. Fault-Scarp Simulation: Generation and Degradation of Topography (MATLAB 'Penck' model of G. E. Hilley and J. Ramon Arrowsmith)

(see MATLAB files on CD that accompanies manual)

Landscape Evolution: Tectonic Uplift, Sea-level Change, and Marine Terrace Generation (MATLAB finite-difference of R. S. Anderson)

```
% seacliff generation  code
% written by r.s. anderson in 1998, with
% modifications since then

% requires the file: delo18.file3
% based on oxygen isotope data from deep-sea cores
% for generation of a sealevel curve

clear
figure(1)
clf
figure(2)
clf
```

```
seamean=-60;
seaamp=60;
% this is the half amplitude of the sealevel change
% period=10000;
pi=3.14159;

% establish time frame, from -740,000 yrs to present (0 yrs)
% use time interval of 100 yrs
tmax=740000;
dt=100;
jmax=(tmax/dt)+1;
jmax
time=0:dt:tmax;
ttmax=max(time);
ttmin=min(time);

% use sin function to generate shape of sea level curve
% sea=seamean+(seaamp*sin(2*pi*time/period));

load delo18.file3;
jj=floor(tmax/2000)+1
a=delo18(1:jj,:);
aflip=flipud(a);
ti=(tmax/1000):-(dt/1000):0;
del=interp1(aflip(:,1),aflip(:,2),ti);
%delmax=max(del)
%delmin=min(del)
delscale=2*seaamp/(4.04)
% sea=seamean-(del*delscale)-2.0792;
% this sets present sea level to zero

sea = -32.841 - (33.747*del)-(8.5605*del.*del);
% this is the nonlinear predictor of sealevel
% (2nd order polynomial)
% derived from scatter plots of del and sea level
% using huon peninsula and bard barbados work 7/14/97

uprate = 0.0005; % uplift rate in m/yr
edot0 = 0.25;
% this is the erosion rate of the sea cliff in m/yr
slope2 = 0.017; % slope of the local shelf

% Can change the following variables:  uplift rate (uprate);
% cliff erosion rate (edot0); and shelf slope (slope2)

dx=5;
```

```
slope = 0.035;
zmin=(seamean-seaamp)-(tmax*uprate)-40
zmax=(seamean+seaamp)+200
%xmax=5000;
xmax=(zmax-zmin)/slope
x=1:dx:xmax;
imax=length(x);
z0=zmin+(slope*x);
z=z0;

kappa0 = 0.015;
% this is the topographic diffusivity in m^2/year

zstar=4;
wavedepth=3*zstar;
% this is the depth to which one will feel waves significantly
dissscale=3*dx*wavedepth;

nprint=40;
jprint=floor(jmax/nprint);
numprint = 0;

%h=plot(x,z);
xplot = x/1000;
xmaxplot = max(xplot);

figure(2)
%subplot(2,1,1)
subplot('position',[.15 .70 .75 .25])
tplot = (time-tmax)/1000;
plot(tplot,sea,'b')
xlabel(['Time (kyr)'],'fontsize',18,'fontname','times')
ylabel(['Sealevel (m)'],'fontsize',18,'fontname','times')
axis([-ttmax/1000 0 -130 20])
set(gca,'fontsize',14,'fontname','times')


%subplot(2,1,2)
subplot('position',[.15 .10 .75 .50])
plot(xplot,z)
axis([0 xmaxplot min(z0) max(z0+(uprate*tmax))]);
%set(h,'erasemode','none');
xlabel(['Distance (m)'],'fontsize',18,'fontname','times')
ylabel(['Elevation (m)'],'fontsize',18,'fontname','times')

zsave=[x;z];
```

```
M = moviein(nprint,gcf);

% ********** start the time clock **********
for j=1:jmax

% the uplift pattern, here taken to be uniform in x
uplift=uprate*dt*ones(1,length(x));
z=z+uplift;
% find the intersection of the sea surface and the topography
surface=sea(j)*ones(1,length(x));
k=find(z>surface);
xsea1(j)=x(k(1));
% here is where we should insert a dependence of the cliff
% erosion rate on the width of the shelf, now ignored
% perhaps decreasing as the weighted water depth
% the most important segments being closest to the instantaneous
% coastline
gg=find(((sea(j)-wavedepth)<z)&(sea(j)>z));
dissrate=exp(-(sea(j)-z(1,gg))/zstar)*dx;
dissipate=sum(dissrate);
edot=edot0*(dissscale/dissipate);
%edot=edot0;
ero(j)=edot;

ksea=k(1)+round(edot*dt/dx);
xsea(j)=x(ksea);
shelf=z(k(1))+(slope2*(x-x(k(1))));

surface(1:(k(1)-1))=9999*ones(size(1:k(1)-1));
surface(ksea+1:imax)=9999*ones(size(ksea+1:imax));
z=min(z,surface);

% now take into account erosion in this reach of
% nearshore area where water depths are < "wavedepth"
ggnew=find(((sea(j)-wavedepth)<z)&(sea(j)>z));
nearshore=wavedepth/(x(max(ggnew))-x(ggnew(1)));
znew=z(1,ggnew(1))+(nearshore*(x(1,ggnew)-x(1,ggnew(1))));
z(1,ggnew)=min(z(1,ggnew),znew);

%now diffuse the terrestrial portion of the space
kappa=zeros(1,length(x));
kkk=find(x>xsea(j));
kappa1=kappa0*ones(1,length(kkk));
kappa(kkk(1):imax)=kappa1;
```

```
dzdt = 4 * kappa .* ((del2(z)./(dx*dx)));
z=z+(dzdt*dt);

%now see if we want to take a snapshot of this
p=rem(j,jprint);
if p == 0
numprint = numprint+1;

figure (2)

%subplot(2,1,1)
subplot('position',[.15 .70 .75 .25])
tplot = (time-tmax)/1000;
plot(tplot,sea,'b')
xlabel(['Time (kyr)'],'fontsize',18,'fontname','times')
ylabel(['Sealevel (m)'],'fontsize',18,'fontname','times')
axis([-ttmax/1000 0 -130 20])
hold on
tnow = (time(j)-tmax)/1000;
plot(tnow,sea(j),'rd','linewidth',3.0)
set(gca,'fontsize',14,'fontname','times')
hold off

        xp1 = xplot;
        xpatch = [0 xp1 xp1(imax:-1:1)];
        zp1 = z;
        zp2 = min(z0)*ones(1,length(x));
        zpatch = [min(z0) zp1 zp2(imax:-1:1)];

        subplot('position',[.15 .10 .75 .50])
%subplot(2,1,2)
plot(xpatch,zpatch,'k');
patch(xpatch,zpatch,'k');

axis([0 xmaxplot min(z0) max(z0+(uprate*tmax))]);
xlabel(['Horizontal Distance (km)'],'fontsize',18,'fontname','times')
ylabel(['Elevation (m)'],'fontsize',18,'fontname','times')
set(gca,'fontsize',14,'fontname','times')

hold on
seanow = sea(j)*ones(1,ksea);
xnowplot = xplot(1:ksea);
plot(xnowplot,seanow,'b','linewidth',3.0)
hold off

%hold on
```

```
zsave=[zsave;z];

edot
abs(time(j)-tmax)

M(:,numprint) = getframe(gcf); % if you dont want movies comment this out
end


end
% ********** now for the plots **********

%plot(x,z,'r')
%set(h,'ydat',z,'color',[0 0 2])

time=time-tmax;
ttmax=max(time);
ttmin=min(time);

seanow = sea(j)*ones(1,ksea);
xnow = x(1:ksea);

figure (1)
subplot(3,1,1)
plot(time,sea,'g')
xlabel('Time (kybp)','fontsize',18,'fontname','times')
ylabel('Sealevel (m)','fontsize',18,'fontname','times')
axis([ttmin/1000 ttmax/1000 -130 20])

subplot(3,1,2)
plot(time,xsea,'r')
xlabel('Time (kybp)','fontsize',18,'fontname','times')
ylabel('Coast (km)','fontsize',18,'fontname','times')
axis([ttmin/1000 ttmax/1000 0 30])

hold on
plot(time,xsea1/1000,'y')
hold off

zzmax=max(z);
zzmin=min(z0);

subplot(3,1,3)
plot(x/1000,z,'k')
axis([0 xmax/1000 zzmin zzmax])
hold on
```

```
plot(x/1000,z0,'r--')
hold on
plot(xnow/1000,seanow,'b')
xlabel('Horizontal Distance (km)','fontsize',18,'fontname','times')
ylabel('Elevation (m)','fontsize',18,'fontname','times')
hold off

zsend=zsave';
save zcliff.file zsend -ascii -tabs

time=time/1000;
erosave=[time;ero]';
save erocliff.file erosave -ascii -tabs

xsea=xsea/1000;
xsave=[xsea;time]';
%save xsea.file xsave -ascii -tabs
% if you want files to manipulate, un-comment this last line

%end

%qtwrite(M,hot,'seacliff',[4 1 5])
% i think this writes a quicktime movie file
% but you can run  the movie by simply typing in the command window:
% figure 3
% clf
% movie(M,3,2) and it'll run the movie 3 times at 2 frames/second
```

REFERENCES

References for Text

Arrowsmith, J.R., and Strecker, M. R., 1999, Seismotetonic range-front segmentation and mountain-belt growth in the Pamir-Alai region, Kyrgyzstan (India-Eurasia collision zone): GSAB, v. 111, no. 11, p. 1,665-1,683.

Bloom, A. L., Broecker, W. S., Chappell, J., Matthews, R. K., and Mesolella, K. J., 1974, Quaternary sea-level fluctuations on a tectonic coast: New $230^{Th}/234$ U dates from the Huon Peninsula, New Guinea: Quaternary Research, v. 4, p. 185-205.

Burbank, Douglas W., and Anderson, Robert S., 2001, Tectonic Geomorphology: Blackwell Science, 274 p.

Bürgmann, Roland, Paul A. Rosen, and Eric J. Fielding, Synthetic Aperture Radar Interferometry to Measure Earth's Surface Topography and its Deformation, Annu. Rev. Earth Planet. Sci. 2000. 28:169-209.

Chappell, J. M., 1983, A revised sea-level record for the last 300,000 years from Papua New Guinea: Search, v. 14, p. 99-101.

Chorley, R.J., 1963, Diastrophic background to twentieth century geomorphological thought: Geological Society of America Bulletin: v. 74, p. 953-970.

Chorley, R.J., Dunn, A. J., and Beckinsale, R. P., 1964, The History of the Study of Landforms, v. I, 678 p., Methuen, New York.

Gomberg, J., and Ellis, M., 1994, Topography and tectonics of the Central New Madrid Seismic Zone: Results of numerical experiments using a 3-D boundary element program: Journal of Geophysical Research, v. 99, p. 20,299-20,310.

King, G. C. P., and Nabelek, John, 1985, Role of fault bends in the initiation and termination of earthquake rupture: Science, 228, p. 984-987.

McManus, Sean, 1998, Digital elevation model analysis applied to active tectonic study in central Asia: M.S. thesis, Arizona State University, 86 p.

Merritts, Dorothy, and Ellis, 1994, Introduction to special section on tectonics and topography: Journal of Geophysical Research, v. 99, n. B6, p. 12,135-12,141.

Merritts, Dorothy, 1996, The Mendocino triple junction: Active faults, paleoseismicity, and causes of rapid uplift: Journal of Geophysical Research (special issue on Paleoseismology), v. 99, no. B7, p. 14,031-14,050.

Merritts, Dorothy J., Bodin, Paul, Beutner, Edward, Prentice, Carol S., and Muller, Jordan, 2001, Active surface deformation in the Mendocino triple junction process zone: *in* Bokelman, Gotz, and Kovach, Robert L. (editors), Proceedings of the 3rd Conference on Tectonic Problems of the San Andreas Fault System, Stanford University Publications/Geological Sciences Volume XXI, September, 2000, pages 128-143. (http://pangea.stanford.edu/GP/sanandreas2000/index.html)

Molnar, Peter, and England, Philip, 1990, Late Cenozoic uplift of mountain ranges and global climate change: chicken or egg? Nature, v. 346, p. 29-34.

Penck, Walther, 1953, Morphological analysis of land forms, trans. By Czech, Hella, and Boswell, Katherine Cumming: London, United Kingdom, MacMillan, 429 p.

Pinter, Nicholas, and Brandon, Mark, 1997, How erosion builds mountain belts: Scientific American, April issue, p. 74-79.

Prentice, Carol S., Merritts, Dorothy J., Beutner, Edward C., Bodin, Paul, Schill, Allison, and Muller, Jordan R., 1999, Northern San Andreas fault near Shelter Cove, California: GSAB, v. 111, no. 4, p. 512-523

Willett, Sean D., Slingerland, Rudy, and Hovius, Niels, 2001, Uplift, Shortening, and Steady State Topography in Active Mountain Belts. American Journal of Science, Vol. 301, pp. 455-485.

Small, Eric, and Anderson, Robert S., 1995, Geomorphically driven Late Cenozoic rock uplift in the Sierra Nevada, California: Science, v. 270, p. 277-280.

Washburn, A., Arrowsmith, J. R., Forman, S. L., Cowgill, E., Wang, X. F., Zhang, Y. Q., and Chen, Z. L., Recent earthquake geology of the central Altyn Tagh Fault, China: Geology, in press, 2001.

References for Table 1

Aitken, M.J., 1998, An introduction to optical dating: the dating of Quaternary sediments by the use of photon-simulated luminescence: Oxford, Oxford University Press, 267 p.

Bada, J.L., 1972, The dating of fossil bones using the racemization of isoleucine: Earth and Planetary Science Letters, v. 15, p. 223-231.

Bada, J.L., Luyendyk, B.P., and Maynard, J.B., 1970, Marine sediments; dating by the racemization of amino acids: Science, v. 170, p. 730-732.

Berger, G. W., 1988, Dating Quaternary events by luminescence, in Easterbrook, D.J., ed., Dating Quaternary sediments: Boulder, Geological Society of America Special Paper 227, p. 13 –50.

Cerling, T.E., and Craig, H., 1994, Geomorphology and insitu cosmogenic isotopes: Annual Review of Earth and Planetary Sciences, v. 22, p. 273-317.

Cox, A., Doell, R.R., and Dalrymple, G.B., 1964, Reversals of the earth's magnetic field: Science, v. 144, p. 1537-1543.

Creer, K.M., 1962, The dispersion of the geomagnetic field due to secular variation and its determination for remote times from paleomagnetic data: Journal of Geophysical Research, v. 67, p. 3461-3476.

Creer, K.M., 1967, Application of rock magnetism to investigations of the secular variation during geological time, magnetism and the cosmos: Univ. Newcastle upon Tyne, NATO Advanced Study Inst. Planetary and Stellar Magnetism, p. 45-59.

Fritts, H.C., 1976, Tree rings and climate: Academic Press, 567 p.

Jacoby, G.C., Jr., Sheppard, P.R., and Sieh, K.E., 1988, Irregular recurrence of large earthquakes along the San Andreas fault: evidence from trees: Science, v. 241.

Ku, T.-L., 1976, The uranium-series methods of age determination: Annual Review of Earth and Planetary Sciences, v. 4, p. 347-379.

Lal, D., 1988, In situ produced cosmogenic isotopes in terrestrial rocks and some applications to geochronology: Annual Reviews of Earth and Planetary Sciences, v. 16, p. 355-388.

Libby, W.F., 1955, Radiocarbon dating: Chicago, University of Chicago Press, 175 p.

Lund, S.P., 1996, A comparison of Holocene paleomagnetic secular variation records from North America: Journal of Geophysical Research, v. 101, p. 8007-8024.

Nishiizumi, K., Winterer, E.L., Kohl, C.P., Klein, J., Middleton, R., Lal, D., and Arnold, J.R., 1989, Cosmic ray production rates of ^{10}Be and ^{26}Al in quartz from glacially polished rocks: Journal of Geophysical Research, v. 94, p. 17, 907-17, 915.

Phillips, F.M., Leavy, B.D., Jannik, N.O., Elmore, D., and Kubik, P.W., 1986, The accumulation of cosmogenic chlorine-36 in rocks; a method for surface exposure dating: Science, v. 231, p. 41-43.

Sarna-Wojcicki, A.M., Lajoie, K.R., Meyer, C.E., Adam, D.P., and Rieck, H.J., 1991, Tephrochronology correlation of upper Neogene sediments along the Pacific margin, conterminous United States, in Morrison, R.B., ed., Quaternary nonglacial geology; conterminous U.S., v. K-2, p. 117-140.

Stuiver, M., 1970, Tree ring, varve and carbon-14 chronologies: Nature, v. 228, p. 454-455.

Wehmiller, J.F., Belknap, D.F., Boutin, B.S., Mirecki, J.E., Rahaim, S.D., and York, L.L., 1988. A review of the aminostratigraphy of Quaternary mollusks from United States Atlantic Coastal Plain sites, in Easterbrook, D.J., ed., Dating Quaternary sediments: Boulder, Geological Society of America Special Paper 227, p. 69-110.

Westgate, J.A., and Gorton, M.P., 1981, Correlation techniques in tephra studies, in Self, S., and Sparks, R.S.J., eds., Tephra Studies: North American Treaty Organization Advanced Studies Institute Series C: Dordecht, Reidel Publishing, p. 73-94.

Yamaguchi, D.K., and Hoblitt, R.P., 1995, Tree-ring dating of pre-1980 volcanic flowage deposits at Mount St. Helens, Washington: Geological Society of America Bulletin, v. 107, p. 1077-1093.